Characterization of Internal Instability Potential of Granular Soils subjected to Uniaxial Static and Cyclic Loading

Jahanzaib Israr[1], Gang Zhang[2] and Jehangir Israr[3]

1. *Department of Civil Engineering, University of Engineering and Technology, Lahore, Pakistan*
2. *School of Civil Engineering and Hydraulic Engineering,, Ningxia University, China*
3. *Water and Sanitation Agency (WASA), Lahore Development Authority (LDA), Pakistan*

* **Corresponding Author:** Email: jisrar@uet.edu.pk

Abstract

Results are reported from a series of hydraulic tests designed to capture the response of soils subjected to simultaneous axial compression and upward seepage flow. An internally stable soil could be characterized by the development of heave at very high hydraulic pressures, while an unstable soil suffered from suffusion at relatively smaller hydraulic pressures. At the onset of seepage failure, the local porosity of critical zone in soil increased, while hydraulic gradients and associated effective stresses decreased. During static tests, seepage induced heave and composite heave-piping failures evolved in dense uniform fine gravels and sands, respectively, and suffusion in gap-graded sand-gravel mixtures. Under cyclic loading, the uniform soils reproduced similar hydraulic responses albeit at relatively smaller applied hydraulic pressures and larger local hydraulic gradients than static tests. The gap-graded soil exhibited premature suffusion that became excessive at higher cyclic frequencies. Cyclic loading induced agitation and transient pore pressure deteriorated the stable constriction network of soil, thereby allowing residual fines to escape from pore spaces and causing internal instability. The instability potential of tested soils could be quantified by comparing the pre- and post-test particle size distribution analyses. Results are compared with the assessments of various existing criteria for internal stability and recommendations are made for possible practical implications.

Key Words: Granular Soils; Geometrical Methods; Internal Instability; Hydraulic Gradient; Relative Density.

1. Introduction

Due to their excellent drainage and stress transfer characteristics, granular soils are used as filtration and drainage layers in various geotechnical infrastructures such as downstream protective filters in embankment dams and subballast layers in railway substructures. In general, filters are expected to arrest the eroding fine particles without clogging to avoid the development of excess pore water pressure in earth structures. While doing so, a filter should not exhibit erosion of their own finer particles (i.e. suffusion) due to seepage forces and disturbance induced by severe mechanical loading, e.g. cyclic loads in railway substructures. The above phenomenon is termed as internal instability and its occurrence can adversely affect the geomechanical characteristics of filters, consequently rendering them ineffective in retaining the protected fine soils, and thereby endangering the structural stability.

Hitherto, numerous empirical criteria have been proposed based on observations from static filtration tests to assess the internal stability of soils, generally ignoring the effects of level of compaction. As pioneers, USACE [1] first examined the role of particle size distribution (PSD) in controlling the inherent or internal stability of soils. The amount of erodible finer fraction was deemed as the most critical factor and empirical threshold values of finer fraction were proposed to control the occurrence of instability.

Kezdi [2] and Sherard [3] applied Terzaghi's [4] filter design criterion to assess the internal stability of granular soils with limited success. Lately, Kenney and Lau [5] experimentally examined the role of PSD curves of soils in greater detail under extreme hydraulic conditions and reported that the shapes of PSD curves controlled the potential for internal instability. Considering that a particle d could only erode through a constriction formed by 4d or larger sized particles, it was proposed that $(H/F)_{min} < 1$will ensure internal stability of soils; where, F is the percentile finer by mass for particle size d, while H is that between d and 4d. Chapius [6] illustrated the similarities of above three criteria and proposed a combined approach based on the slope of soil's particle size distribution curve (PSD). Notably, the existing approaches including above were based on PSD of soils and they do not

consider any hydraulic and physical factors, e.g. hydraulic gradients, loading conditions, and relative density of soils etc. Burenkova [7] proposed a semi-empirical criterion, which assumed that when the finer fraction is mixed with a coarser fraction it does not form part of the basic soil skeleton if it does not cause an increase in volume. Using particle sizes d_{15}, d_{60} and d_{90}, the concept of conditional factors of uniformity, $h' = d_{90}/ d_{60}$ and $h'' = d_{90}/d_{15}$ proposed to quantify the homogeneity and hence the internal stability of soils. Boundaries were proposed in the form of contours separating internally stable and unstable soils in a plane formed by the factors h' and h''. Lately, Wan and Fell [8] performed more experiments on silt-sand and sand-gravel mixtures and modified the boundaries proposed by Burenkova [7].

Indraratna et al. [9] analyzed a large experimental database of existing and new hydraulic test results and proposed a constriction size distribution (CSD) based technique to capture the effects of relative density on internal stability of soils. For brevity, the proposed technique combines the method of Kenney and Lau [5] with the CSD based filter design criterion of Indraratna et al. [10], whereby the PSD curve of soil is demarcated at a point corresponding to $(H/F)_{min}$ to yield an arbitrary coarser "filter" and a finer "base" soil fractions (Fig. 1). The next step requires one to draw the CSD of filter fraction and the PSD of base fraction by using the surface area techniques. Finally, if the given arbitrary filter satisfies the criterion of Indraratna et al. [10] in protecting the finer base fraction, the soil gradation is deemed internally stable.

This study purports to experimentally evaluate the important physical and hydraulic factors affecting the internal instability potential of granular soils such as density, particle gradation, hydraulic gradients, and mechanical loading (both static and cyclic) . Accordingly, results are reported from an experimental program having 3 test phases; namely I, II, and III, with 61 hydraulic tests conducted on 10 soils under no-load, static loads and cyclic loads, respectively. During phase-I, a total of 24 tests were performed to assess the role of PSD and relative density (Rd) in controlling the internal stability of soils. The later testing phases were designed to simulate the practical conditions such as the downstream filters in dams under normal stresses and the subballast filters in railway substructure under heavy haul cyclic loading during the next two phases-II and III, respectively. During phase-II, the effects of varying the effective stress magnitude on internal stability potential were evaluated through 15 hydraulic tests. Similarly, phase-III examined the effects of cyclic loading frequency through 22 additional hydraulic tests. The test results of phases-II and III were then compared to evaluate the effects of cyclic loading on extent of internal erosion potential and seepage failure modes. Nevertheless, the experimental results of this study could be used to evaluate and improve upon the well-accepted CSD based geometrical method.

2. Laboratory Program

2.1 Test Material and Setup

As Fig. 2 shows, the material for testing included a total of 10 non-cohesive granular soils, i.e. three uniform soils namely A1, A2 and A3, two well-graded soils B1 and B2, three broadly-graded soils C1, C2 and C3 and two gap-graded soils D1 and D2. The testing material consisted of uniform medium sands, uniform fine gravel, and non-uniform sand-gravel and clay-silt-sand-gravel mixtures with negligible plasticity.

Table 1 summarizes the physical characteristics of current test samples. Notably, the selected soil gradations plot within the typical subballast filter selection range in New South Wales, Australia [11, 12]. Moreover, some of these soils also conform to the materials commonly used as downstream filters and transition layers in embankment dams [10, 13, 14].

As shown in the inset of Fig. 2, the test chamber consisted of a low friction polycarbon cell with a diameter of 240 mm and height of 300 mm. The apparatus was large enough to yield size ratio, R (i.e. cell diameter/ maximum particle size) > 12, which were deemed sufficient to avoid the effects of boundary and instrumentation on soil erosion plus the development of preferential flow paths [15].

The seepage induced variations in porosity, head losses and effective stress were captured using arrays of 3 porometers, 8 pore pressure transducers, and 3 load sensors probed at different depths, respectively. Further details on apparatus, performance and test repeatability are provided elsewhere by Israr and Israr [16].

2.2 Sampling and Compaction

The 200 mm long specimens were compacted in 5 layers to the target relative density (R_d) by controlling the dry soil mass and using the predetermined limiting void ratios e_{min} and e_{max} (Table 1). The uniformity of samples with respect to compaction and particle distribution was

ensured through preliminary trials, following procedure of Indraratna et al. [9]. For instance, several trial specimens were obtained using hand compaction of Skempton and Brogan [17], rod compaction of Indraratna et al. [9] and the standard compaction techniques to achieve the target relative densities between 0% and 100%. Samples at intermediate $R_d \approx 30\%$, 50%, 60% and 70% were compacted by a 0.75 kg steel rod (300 mm long and 20 mm diameter). Nevertheless, the imparted compaction energies were computed to be 26, 157, 263, 313, 364, 564 kJ/m^3 for $R_d \approx 5\%$, 30, 50, 60, 70 and 95, respectively [9, 18].

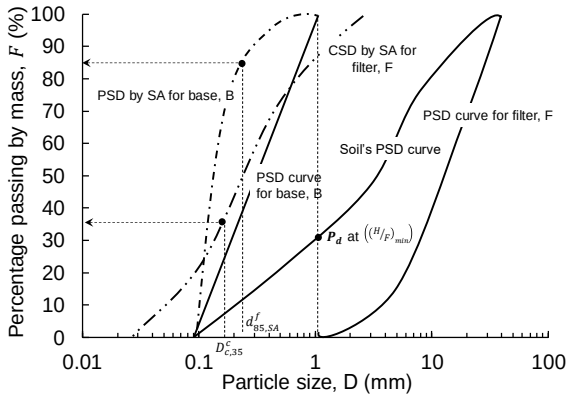

Fig. 1: Illustration of CSD based method: discretization of soil's PSD into a coarser fraction F and finer fraction B to determine controlling constriction and representative base particle sizes by surface area technique

2.3 Saturation and Consolidation

The specimens were carefully saturated for 24 to 48 hours after de-airing them using the back pressures of up to 120 kPa. The Rd was kept ≥ 95% during phases-II and III, and the specimens were consolidated under the target normal stress before the hydraulic testing. The target loads were applied using a computer-controlled dynamic actuator that could apply cyclic loads for a range of frequencies between 0 and 40 Hz. A hydraulic piston mounted on a fixed frame transmitted the required loads to the specimens through a metallic shaft connected to the flexible loading platen (±0.1% accuracy). Note that the metallic shaft passes through the top boundary of hydraulic chamber inside a frictionless seal with negligible contact stress reduction (< 1%). To simulate static normal stresses, the frequency was set to zero and the rate of loading was kept slow enough to avoid the development of pore water pressure while target normal static stresses of 25, 50 and 100 kPa being applied prior to testing during phase-II.

During cyclic tests of phase-III, a sinusoidal stress pattern with σ_{min}' =30 kPa,σ_{max}' =70 kPa,and σ_{mean}' = 50 kPa was applied to replicate a subballast filter under heavy-haul train loading. Following static loading procedure, an initial stress of σ_{min}' = 30 kPa was monotonically applied before the application of cyclic deviator stress of 40 kPa. In this study, cyclic loading frequencies of 5, 10, 20 and 30 Hz (i.e. up to 210 km/hr) over a large number of loading cycles (up to 1.55 million) were simulated. Further details on the loading system are given elsewhere by Israr et al. [11] and Trani and Indraratna [19].

2.4 Test Procedure and Rationale

The upward flow was applied from the bottom at controlled pressure and then increased in small steps to the critical onset of failure, which was characterized by visual piping, heave or effluent turbidity > 60 NTU [9]. The increments in hydraulic pressure and hence the hydraulic gradient *i* were kept small enough such that the accurate value of observed i_{cr} may be determined when seepage failure commenced. For example, for narrow gradations A and B, the increments of *i* were kept smaller than 0.05, while for broad gradations C and D, these increments were kept below 0.025. The test duration at a certain value of *i* lasted up to 30 minutes beyond which steady state flow commenced and the next increment of *i* could then be applied for a subsequent stage. In lieu of mass loss, this threshold of 60 NTU was observed to be an acceptable measure of significant suffusion [20]. The onset of instability or failure could be identified by; (i) significant variations of flow curves given by effluent flow rate versus hydraulic gradient, (ii) sudden drop in the magnitude of hydraulic gradient, (iii) visual evidence of piping, heave or effluent turbidity > 60 NTU for a period of 30 minutes or more. Further increase in hydraulic pressure beyond the critical onset significantly increased the erosion of fines, while the hydraulic gradient dropped. At this critical onsets, the average and local hydraulic gradient magnitudes were considered as critical and are denoted by $i_{cr,a}$ and $i_{cr,ij}$, respectively, in this study. Here, the $i_{cr,a}$ was determined from the head loss between inflow (P0) and outflow (P7) transducers, while the $i_{cr,ij}$ could be obtained from the differential head between the two adjacent local pore pressure transducers (Fig. 2). To allow for better commissioning, control over test data, repeatability and lesser potential disturbance to the test specimens, the local transducers were not employed and only the $i_{cr,a}$ values were monitored during phase-I.

Table 1: Characteristics of current samples including identity, physical properties and soil description

ID	C_u	R_g	e_{min}	e_{max}	$i_{cr,\,th}$	Soil description
A1	1	--	0.41	0.76	1.19	Uniform medium sand
A2	1.2	--	0.39	0.74	0.97	
		--	0.39	0.74	1.07	
		--	0.39	0.74	1.18	
A3	1.5	--	0.42	0.78	1.21	Uniform fine gravel
B1	5	--	0.37	0.76	0.94	Well-graded gravelly-sand
		--	0.37	0.76	1.03	
		--	0.37	0.76	1.13	
B2	10	--	0.36	0.75	0.93	
		--	0.36	0.75	1.01	
		--	0.36	0.75	1.12	
C1	20	--	0.32	0.75	0.92	Broadly-graded gravelly- sand
		--	0.32	0.75	1.02	
		--	0.32	0.75	1.07	
		--	0.32	0.75	1.14	
C2	23	--	0.31	0.73	0.93	
		--	0.31	0.73	0.98	
		--	0.31	0.73	1.05	
		--	0.31	0.73	1.13	
C3	40	--	0.33	0.77	0.92	
		--	0.33	0.77	1.02	
		--	0.33	0.77	1.14	
D1	20	5	0.36	0.78	1.1	Gap-graded gravelly sand
D2	304	10	0.37	0.78	1.12	Gap-graded silt-sand-gravel mixture

Note: C_u = uniformity coefficient, R_g = gap ratio, R_d = relative density (%), e_{min} = minimum void ratio, e_{max} = maximum void ratio, and $i_{cr,\,th}$ = theoretical critical hydraulic gradient [4].

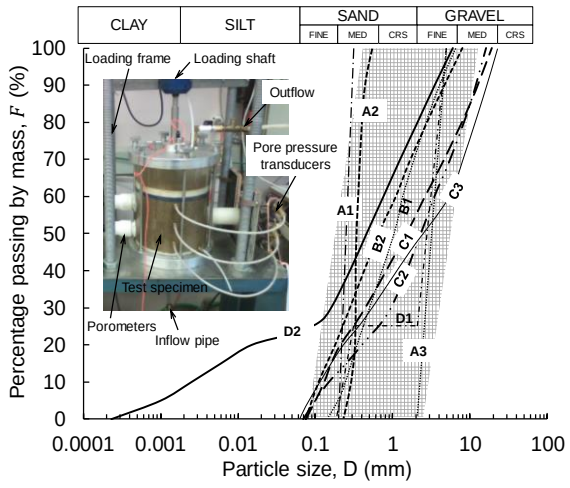

Fig. 2: Particle size distributions of soils investigated (**Note**: shaded region is the typical subballast filter selection range in NSW, Australia [12])

However, complete instrumentation (3 porometers, 2 load cells, 6 internal pore pressure transducers) was installed during later phases-II and III and no significant differences were observed in specimen behaviour in either phases. The tested specimens were then retrieved in 5 distinct soil layers for post-test analysis to determine any changes in their PSD curves as a result of erosion. As an acceptable indication of internal instability potential, the erosion was quantified as the dry mass of the finer fraction washed from the test samples and deposited in the sedimentation tank [20]. The erosion or loss of finer fraction, expressed as a percentage of the original dry mass of samples, would permanently alter the original shape of PSD curve of an internally unstable soil [5].

3. Test Results and Discussion

3.1 Hydraulic Response of Soils under Gravity Loading

Fig. 3 shows the variations of effluent flow rate and turbidity with the average hydraulic gradient (i_a), whereby critical onsets could be clearly identified by variations in the slopes of the flow and turbidity curves. Due to the increase in Rd of soil A2, the effluent flow rate decreased and the magnitude of applied critical hydraulic gradient ($i_{cr,a}$) increased, while the effluent turbidity remained well-below 60 NTU until the critical onset of heave. Similarly, the slopes of flow and turbidity curves markedly decreased with

the increase in R_d of other soils B2, C1 and C3, as shown in Figs. 3b, 3c and 3d, respectively. The seepage induced failures in soils A, B, C3 and D remained quite consistent and somehow independent of level of compaction. For instance, the onset of heave in soils A and B observed at $i_{cr,a} \geq 1$, while that of suffusion in soils C3, D1 and D2 at $i_{cr,a} \ll 1$. Nevertheless, the broadly-graded soils C1 and C2 exhibited dramatic change in their seepage induced response, whereby the inception of suffusion (i.e. excessive erosion) at lower levels of compaction transformed to the development of heave at $i_{cr,a} \approx 1$ with no or limited erosion. Similarly, the response of soil D2 observed to be consistent Fig. 4 illustrates the occurrence of seepage induced failures in some of the selected samples. For example, sample B2 in its loosest state of compaction still exhibited heave failure at $i_{cr,a} > i_{cr,th}$, while the failure mode changed from composite suffusion-piping at smaller $i_{cr,a}$, to heave-piping at larger $i_{cr,a}$, for broadly-graded sample C1. Nonetheless, the failure mechanism for sample D2 could not be altered by increasing the R_d that still suffered from suffusion at level compaction levels. As shown in Fig. 5, increasing the R_d of test samples could significantly decrease the internal erosion and increase the magnitudes of $i_{cr,a}$, especially in the borderline broadly-graded soils C1 and C2.

3.2 Hydraulic Response under Static Loading

As shown in Figs. 6a and 6b, increase in the static loading magnitude proportionally increased the icr,a, and decreased the associated effluent turbidity until reaching the critical onsets of heave in soils B2 and D2, as identified by sudden rise in the slopes of flow and turbidity curves. It may be attributed to the increased effective contact stresses at particle level at higher magnitudes of static load that incurred greater hydraulic head losses while mobilizing the particles, e.g. see [21]. This is also fully consistent with Terzaghi's [4] laboratory observations and the recommendations of Skempton and Brogan [17] on loaded or inverted downstream protective filters. This increase in the magnitude of icr,a, was higher in samples with linear gradations, e.g. soils A and B, while the same was less significant in samples with non-linear gradations, i.e. soils C and D. For instance, icr,a for well graded-soil B2 escalated from nearly one to 55, when the magnitude of normal effective stress increased from 0 to 100 kPa (Fig. 7). In contrast, the value of icr,a for gap-graded soil D2 barely increased from 0.37 at 0 kPa to 25 at 100 kPa. Nevertheless, before the occurrence of suffusion in D2 under static loading, the shapes of flow curves remained identical and the associated effluent turbidity well below 60 NTU that could also verify the repeatability of hydraulic testing. Given the rate of static load application was kept very slow, no significant pore pressure developments observed during tests in phase-II. An analysis of pre- and post-test samples revealed that the relative density of tested samples did not change, although the PSD curves of internally unstable samples showed significant changes due to erosion of finer fraction, while PSD of a stable sample remained unaltered.

3.3 Hydraulic Response under Cyclic Loading

Fig. 6c and 6d shows that the flow curves for samples B2 and D2 subjected to cyclic loading were less steeper than those obtained during static tests (see previous Fig. 6a) in the pre-critical regime (ia < icr,a). The densification due to cyclic loading during initial 40,000 to 100,000 cycles reduced the permeability of test samples. The magnitudes of critical hydraulic gradient icr,a continued to decrease with increase in loading frequency for both soils B2 and D2. Interestingly, soil B2 still exhibited no significant erosion and the development of heave failure observed at very large hydraulic gradients compared to soil D2, hence proving to be internally stable under severe cyclic conditions. Nevertheless, the blatant agitation due to dynamic loading did not allow the stable constriction network to retain the finer particles of soil D2 and they continued to erode even at very small ia-values, as indicated by the turbidity curves (turbidity >> 60 NTU) in Fig. 6d. During static tests, the time histories of local porosity variations for soils B2 and D2 remained generally uniform before the inception of heave and suffusion, respectively (Figs. 8a-8b). In contrast, rapid compression due to cyclic densification observed in the first 20 minutes of testing under cyclic conditions, where porosity of test samples abruptly decreased. The response of internally stable sample D2 remained uniform (i.e. no porosity variations) before the inception of heave that clearly indicated no significant intern-particle movements and erosion prior to the development of heave (Figs. 8b and 8d). In contrast, the unstable sample D2 showed continuous deteriorations in local porosity due to significant inter-particle movements and internal erosion, which became excessive at the onset of suffusion and beyond (Figs. 8b and 8d). Nevertheless, similar initial porosity values of test samples during static and cyclic tests clearly indicated higher degree of specimen uniformity and acceptable test repeatability.

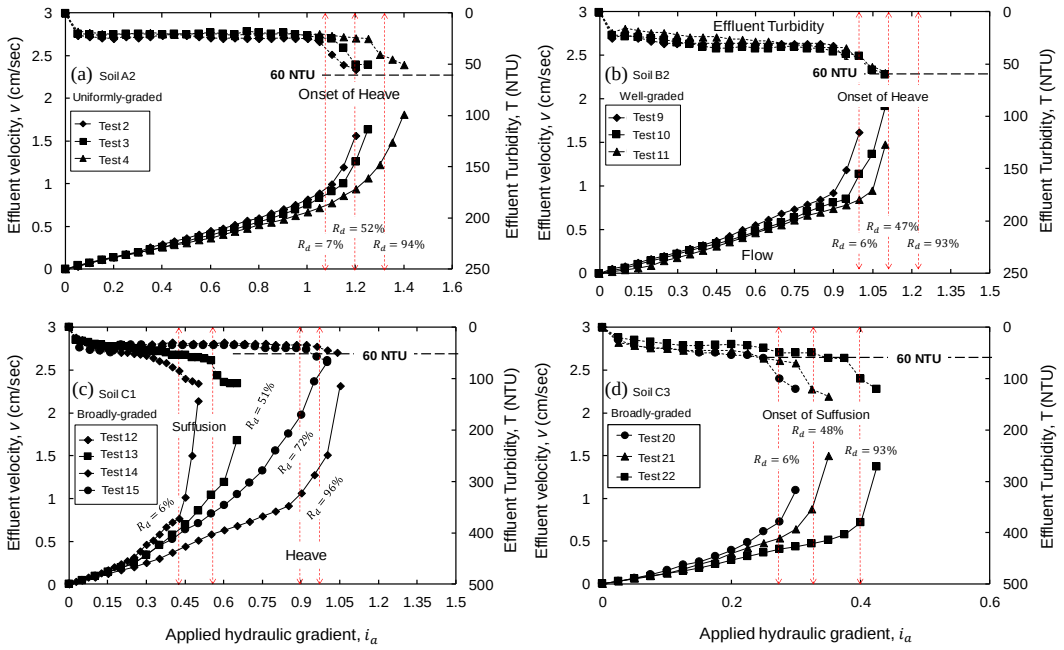

Fig. 3: Hydraulic test results for selected samples A2 and C3 during phase-I

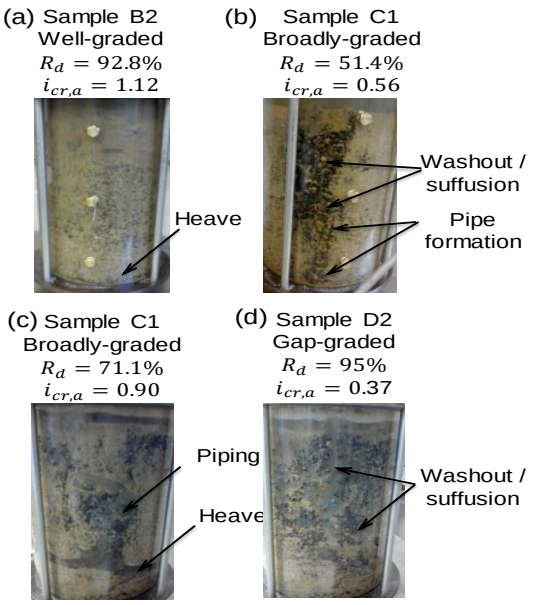

Fig. 4: Seepage failures observed in phase-I

Fig. 9a and 9b show the comparisons between the effects of static loading magnitude and cyclic frequency on seepage responses of selected samples. As a result of increase in static loading magnitude from 0 to 100 kPa, the magnitude of $i_{cr,a}$ increased, while internal erosion decreased (Fig. 9a), thus increasing the stability of specimens. This could be attributed to the increased effective stress on eroding particles, hence requiring higher hydraulic gradients to dislodge them from pore spaces. Interestingly, the well-graded sample B2 (C_u=10) exhibited negligible erosion and plotted over the highly stable uniformly-graded soils A1 and A3, thereby indicating a higher degree of internal stability and suitability as a protective filter. Nevertheless, under cyclic loading, the magnitudes of $i_{cr,a}$ decreased, while the internal erosion increased with the increase in loading frequency. For example, the internal erosion at 0 Hz nearly doubled at 30 Hz for all test samples because of the agitation due to cyclic loading, which disturbed the stable constriction network and allowed fines to escape.

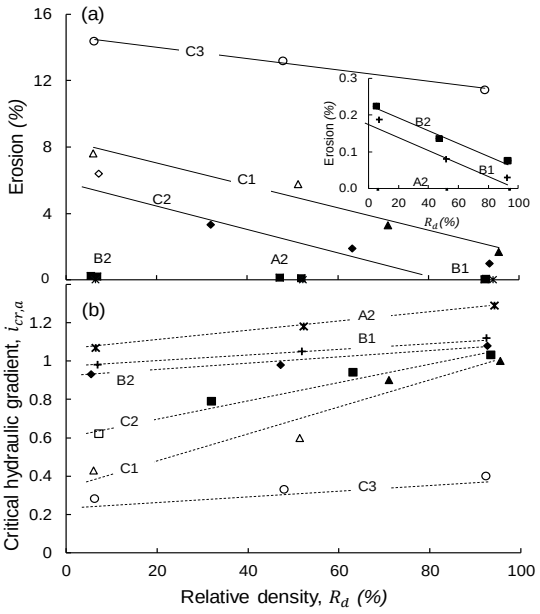

Fig. 5: Effects of R_d on (a) Internal erosion and (b) critical hydraulic gradients

Table 2: Summary of laboratory test results of phase-I (Gravity Loading Tests)

No	ID	Prior Assessments of Internal Stability						R_d (%)	Seepage failure	EX[#]
		IE	KZ	KL	SH	WF	BK			
1	A1-R96	S	S	S	S	S	S	96	Heave	S
2	A2-R6	S	S	S	S	S	S	6.6	Heave	S
3	A2-R52	S	S	S	S	S	S	52	Heave	S
4	A2-R94	S	S	S	S	S	S	94	Heave	S
5	A3-R95	S	S	S	S	S	S	95	Heave	S
6	B1-R7	S	S	S	S	S	S	7	Heave	S
7	B1-R52	S	S	S	S	S	S	52	Heave	S
8	B1-R93	S	S	S	S	S	S	93	Heave	S
9	B2-R6	S	S	S	S	S	S	6	Heave	S
10	B2-R47	S	S	S	S	S	S	47	Heave	S
11	B2-R93	S	S	S	S	S	S	93	Heave	S
12	C1-R6	U	S	S	S	S	S	6	Suffusion	U
13	C1-R51	U	S	S	S	S	S	51	Suffusion	U
14	C1-R72	S	S	S	S	S	S	72	Composite*	S
15	C1-R96	S	S	S	S	S	S	96	Heave	S
16	C2-R7	U	U	S	U	S	S	7	Suffusion	U
17	C2-R32	S	U	S	U	S	S	32	Composite*	S
18	C2-R63	S	U	S	U	S	S	63	Composite*	S
19	C2-R94	S	U	S	S	S	S	94	Heave	S
20	C3-R6	U	U	U	S	U	U	6	Suffusion	U
21	C3-R48	U	U	U	S	U	U	48	Suffusion	U
22	C3-R93	U	U	U	S	U	U	93	Suffusion	U
23	D1-R95	U	U	U	U	U	U	95	Suffusion	U
24	D2-R95	U	U	U	U	U	U	95	Suffusion	U

[#] Experimental observations
[*] A composite of heave, piping and suffusion failure evolving in the specimen

Table 3: Summary of laboratory test results of phase-II (Static Loading Tests)

No	ID	Prior Assessments of Internal Stability						σ'_{vt}* (kPa)	R_d (%)	Seepage failure	EX
		IE	KZ	KL	SH	WF	BK				
25	A1	S	S	S	S	S	S	50	96	Heave	S
26	A3	S	S	S	S	S	S	50	96	Heave	S
27	B2	S	S	S	S	S	S	25	96	Heave	S
28	B2	S	S	S	S	S	S	50	97	Heave	S
29	B2	S	S	S	S	S	S	100	96	Heave	S
30	C1	U	S	S	S	S	S	25	98	Suffusion	U
31	C1	S	S	S	S	S	S	50	97	Heave	S
32	C1	S	S	S	S	S	S	100	96	Heave	S
33	C2	U	U	S	S	S	S	25	98	Suffusion	U
34	C2	S	U	S	S	S	S	50	96	Heave	S
35	C2	S	U	S	S	S	S	100	95	Heave	S
36	D1	U	U	U	U	S	S	50	97	Suffusion	U
37	D2	U	U	U	U	S	S	25	98	Suffusion	U
38	D2	U	U	U	U	S	S	50	99	Suffusion	U
39	D2	U	U	U	U	S	S	100	98	Suffusion	U

[*] Applied normal effective stress (kPa)

Previous studies revealed that the internal erosion majorly occurs in the first 40,000 to 100,000 loading cycles before the shakedown occurs [22, 23]. As Fig. 10b shows, the internal erosion becomes less significant beyond 0.5 million load cycles. The analysis of pre- and post-

test samples revealed that the final R_d was 100%, which is attributed to the effects of cyclic densification. For internally stable samples with no erosion, cyclic densification results into 100% relative density in the first few thousand cycles [11], e.g. there is barely any increase in erosion for sample B2, no matter at 5Hz or 30 Hz. Note in this study, only the physical effects of agitation and pore pressure developments due to cyclic loading were considered without quantifications. For instance, the agitation due to cyclic loading did not allow the stable constrictions to sustain and the excess pore pressures triggered pre-mature internal erosion (i.e. suffusion) at increasingly smaller $i_{cr,a}$, at higher loading frequencies, as shown in previous Fig. 7b. Under cyclic loading, all current soils exhibited marked deterioration in their respective $i_{cr,a}$-values due to the development of excess pore water, when the cyclic frequency increased from 0 to 30 Hz.

3.4. Experimental Observations on Internal Stability

The current rationale to characterize an internally stable specimen included: (i) unaltered shape and C_u value of PSD curve for a specimen, (ii) less than 4% internal erosion of fines, and (iii) development of heave at $i_{cr} \geq i_{ct}$ from classical piping theory [5, 9, 17]. Summary of test results from each testing phase is presented through Tables 2, 3 and 4. The analysis revealed that only specimens D1 and D2 showed internal instability under static conditions, whereas the rest could be characterized as internally stable. However under cyclic loading, specimens C1, C2, C3, D1, and D2 showed internal instability.

4. Seepage Failures in Stable and Unstable Soils

Fig. 10 illustrates the types of seepage failures in selected samples under both static and cyclic loading. The well-graded specimen (B2) exhibited heave failure with no erosion and therefore remained internally stable at all relative densities. The broadly-graded specimens (C1 and C2) showed internal stability only at higher compaction levels, i.e. heave development at $i_{cr,a} \approx i_{cr,th}$ of Terzaghi [4] and unaltered PSD curves with less than 4% erosion [22]. Nonetheless, the gap-graded soil D2 suffered from suffusion at all compaction levels, although the amount of erosion reduced with the increase in Rd. Similarly, the magnitudes of i_{cr} increased and that of erosion decreased with the increase in magnitude of static loading. In summary, all specimens showed enhanced stability at higher R_d under static loading except the gap-graded soils, which failed to show internal stability.

Abrupt compressions of samples were recorded due to cyclic densification that incurred permeability reductions. Additionally, the cyclic loads imparted physical disturbance to the specimens in the form of agitation and generated the pore pressure due to low permeability, thereby reducing effective stress. The constriction network of coarse fraction could not maintain its stability, hence allowing drag and hydrodynamic forces to trigger erosion of fines from the pore spaces. The internal erosion became excessive at higher frequencies, whereby none of the specimens showed internal stability under cyclic loading except soils A1-A3 and B1-B2 (Table 4). The analysis revealed that the response of a compacted ($R_d \geq 95\%$) specimen under cyclic loading became similar to that of a loose specimen ($R_d < 5\%$) under static conditions. Fig. 11a-11e illustrate the generalized mechanisms for two types of seepage failures in granular soils. Fig. 11b shows that an internally stable soil exhibits heave development at $i_{cr,a} \geq i_{cr,th}$ that occasionally accompanied by some limited erosion, depending upon the soil type, e.g. fully compacted B1 and B2 showed composite heave-piping failures. At the critical onset of heave, an internally stable specimen is lifted up like a rigid soil column by the hydraulic forces, resulting into occasional volume changes. The seepage and buoyant forces neutralize the effective stresses and boundary or skin friction (Fig. 11c), thereby allowing the whole specimen to move as an entity. No or very limited erosion (under dynamic conditions) with unaltered post-test PSD curves indicate that the inter-particle arrangement remains intact during the occurrence of heave, where boundary friction from cell walls may play an important role.

As Fig.11d shows, an internally unstable soil suffers from suffusion at critical hydraulic gradients smaller than that for quick sand condition, i.e. $i_{cr,th} = \gamma_s / \gamma_w = 1$; where γ_s and γ_w define the unit weights of soil and water, respectively [4]. The washout of fines incurs changes in original PSD of soils, thereby making it more porous. The post-test forensic analysis revealed that the washed fraction comprised of fine and medium sand particles smaller than the controlling constriction sizes of coarse fractions. During instability, the coarse particles remain intact (i.e. stable), while the effluent accompanies the fine particles from the pore spaces without causing reductions in specimen volume. The specimen boundary conditions do not influence the process of erosion in internally unstable soils,

where the inter-particle friction plays a more significant role (Fig. 11e).

5. Geometrical Assessments

5.1 Existing Approaches

All current specimens were re-examined using two well-accepted PSD based and a CSD based geometrical criteria, as shown in Tables 2, 3 and 4. Note that a geometrical approach referred herein is the one that considers the shapes of PSD and CSD curves of soils to determine its susceptibility to internal instability. The acronyms KL, KZ, BK, SH, WF and IE define the criteria from Kenney and Lau [5], Kezdi [2], Burenkova [7], Sherard [3], Wan and Fell [8], and Indraratna et al. [9], respectively. The analysis of test results from phase-I revealed that the criteria of KL, KZ, BK, SH and WF yielded 3, 5, 3, 7 and 3 inconsistent predictions, respectively (Table 1). Given that the level of compaction was varied during this phase, the above PSD based criteria failed to capture its effects in borderline specimens C1 and C2. As a result of increase in R_d, the constrictions become increasingly finer and consequently retain the characteristic particle size of the finer fraction to initiate the process of local self-filtering [14].

Not surprisingly, the IE criterion, which is equally sensitive to the PSD and R_d of soils, assessed the current test results with 100% success. During phase-2, the PSD criteria showed insensitivity to the static loading magnitude, where the criteria of KL, KZ, BK, SH and WF resulted into 2, 3, 6, 2 and 6 inconsistent predictions, respectively. However, the predictions from IE agreed fully with the current EXP results (Table 3). Table 4 presents the results of internal stability assessments for test specimens subjected to cyclic loading. Unlike the predictions for static tests, none of the existing criteria showed 100% success. For instance, KL, KZ, BK, SH, WF and IE yielded 8, 4, 16, 8, 16 and 8 inconsistent predictions, respectively. The agitation and companion pore water pressure generated due to cyclic loading deteriorated the stable constriction network of primary fabric, consequently allowing the fines to escape with the effluent (i.e. suffusion). Note that the geometrical approaches described previously do not capture this constriction deterioration mechanism, thereby resulting into inconsistent assessments. In this study, the existing CSD based approach of Indraratna et al. [9] is modified to capture these effects of cyclic loading; namely modified Indraratna et al. criterion or MIE.

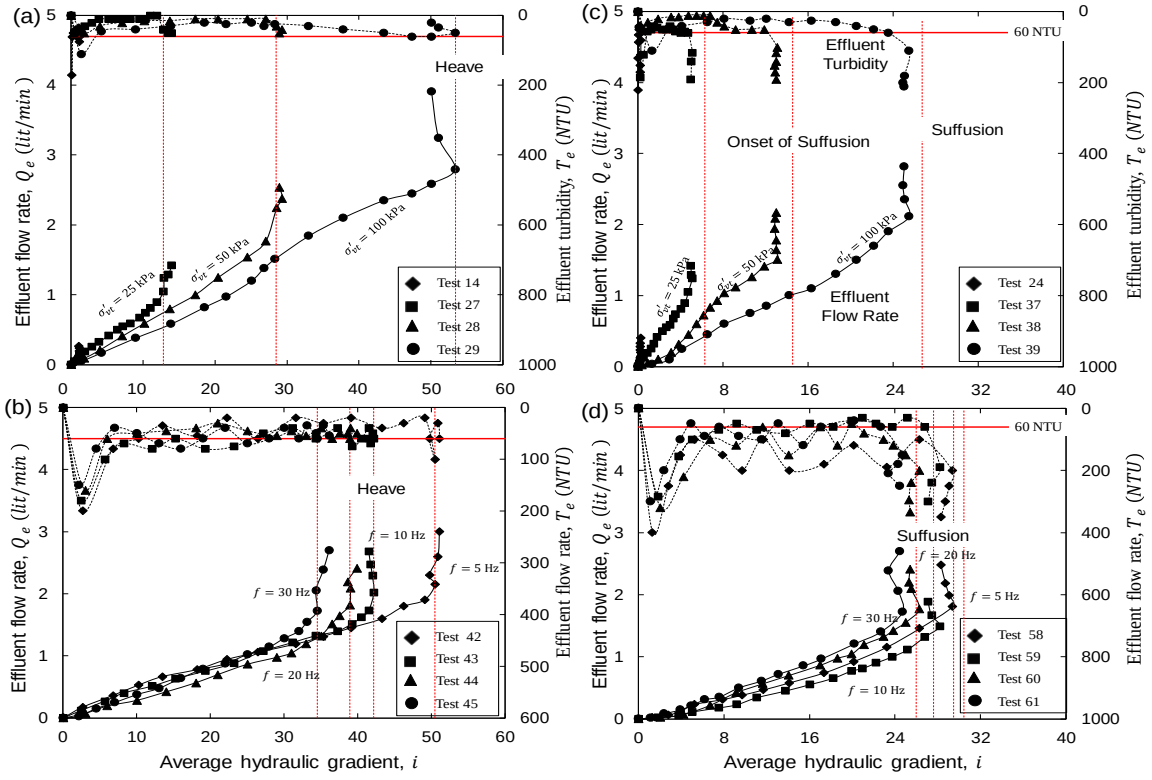

Fig. 6: Hydraulic results for selected samples under (a) static loading and (b) cyclic loading

Table 4: Summary of laboratory test results of phase-III (Cyclic Loading Tests)

No	ID	Prior Assessments of Internal Stability						*f* * (Hz)	R_d (%)	Seepage failure	EX	MIE
		IE	KZ	KL	SH	WF	BK					
40	A1	S	S	S	S	S	S	5	97	Heave	S	S
41	A3	S	S	S	S	S	S	5	96	Heave	S	S
42	B2	S	S	S	S	S	S	5	97	Heave	S	S
43	B2	S	S	S	S	S	S	10	97	Heave	S	S
44	B2	S	S	S	S	S	S	20	96	Heave	S	S
45	B2	S	S	S	S	S	S	30	98	Heave	S	S
46	C1	S	S	S	S	S	S	5	97	Suffusion	U	U
47	C1	S	S	S	S	S	S	10	96	Suffusion	U	U
48	C1	S	S	S	S	S	S	20	97	Suffusion	U	U
49	C1	S	S	S	S	S	S	30	98	Suffusion	U	U
50	C2	S	U	S	S	S	S	5	98	Suffusion	U	U
51	C2	S	U	S	S	S	S	10	97	Suffusion	U	U
52	C2	S	U	S	S	S	S	20	96	Suffusion	U	U
53	C2	S	U	S	S	S	S	30	98	Suffusion	U	U
54	D1	U	U	U	U	S	S	5	96	Suffusion	U	U
55	D1	U	U	U	U	S	S	10	97	Suffusion	U	U
56	D1	U	U	U	U	S	S	15	97	Suffusion	U	U
57	D1	U	U	U	U	S	S	20	96	Suffusion	U	U
58	D2	U	U	U	U	S	S	5	97	Suffusion	U	U
59	D2	U	U	U	U	S	S	10	98	Suffusion	U	U
60	D2	U	U	U	U	S	S	20	99	Suffusion	U	U
61	D2	U	U	U	U	S	S	30	99	Suffusion	U	U

* Applied cyclic loading frequency (Hz)

Table 5: Summary of laboratory data adopted from literature for the verification of proposed criterion

ID	Sources	Prior Assessments of Internal Stability			*f* (Hz)	Cyclic Load*	Seepage failure	EX	MIE
		IE	KL	KZ					
Kb-15(F)	Kabir et al. [24]	U	S	S	2	70/140	--**	S	S
Kb-15(F)		U	S	S	10	70/140	Suffusion	U	U
Kb-B(1)		U	U	U	2	70/140	Suffusion	U	U
Kb-B(2)		U	U	U	10	70/140	Suffusion	U	U
H-12(1)	Haque et al. [13]	U	S	U	2	75/140	--**	S	S
H-12(2)		U	S	U	5	75/140	--**	S	S
H-12(3)		U	S	U	10	75/140	Suffusion	U	U
H-12(4)		U	S	U	15	75/140	Suffusion	U	U
Km-15(1)	Kamruzzaman et al. [23]	S	S	S	10	70/140	--**	S	S
Km-15(2)		S	S	U	10	70/140	--**	S	S
Km-15(3)		U	S	U	10	70/140	Suffusion	U	U
Km-15(4)		U	U	U	10	70/140	Suffusion	U	U
Km-25		U	U	U	10	70/140	Suffusion	U	U
Km-45		U	U	U	10	70/140	Suffusion	U	U
F-5	Trani [12]	U	U	U	5	30/70	Suffusion	U	U
T-01		S	U	U	5	30/70	Suffusion	U	U
T-02		S	S	S	5	30/70	Suffusion	U	U
T-03		S	S	S	5	30/70	--**	S	S
F-1	Trani and Indraratna	S	S	S	5	30/70	--**	S	S
F-2		S	S	S	5	30/70	Suffusion	U	U

F-3	[19]	S	S	S	5	30/70	--**	S	S
F-4		U	S	S	5	30/70	Suffusion	U	U
C-12(1)	Ip. et al. [25]	S	S	U	5	70/140	--**	S	S
C-12(2)		S	S	U	5	70/140	--**	S	S
C-12(3)		S	S	U	5	70/140	--**	S	S
C-12(4)		S	S	U	5	70/140	--**	S	S
C-12(1)		S	S	U	10	70/140	--**	S	S
C-12(2)		S	S	U	10	70/140	--**	S	S
BS	Alobaidi and Hoare [26]	S	S	S	0.5	--	--**	S	S
BS		S	S	S	2	--	--**	S	S

* Numerator and denominator represent minimum and maximum cyclic stress (kPa), respectively
** No information reported

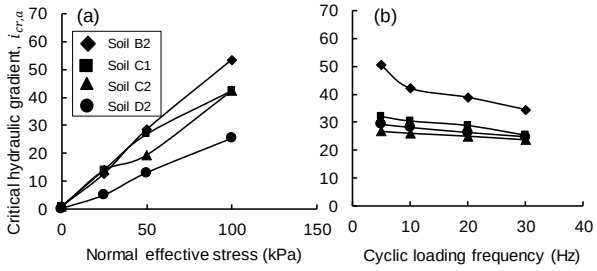

Fig. 7: Effects of (a) normal static load and (b) cyclic loading frequency on $i_{cr,a}$

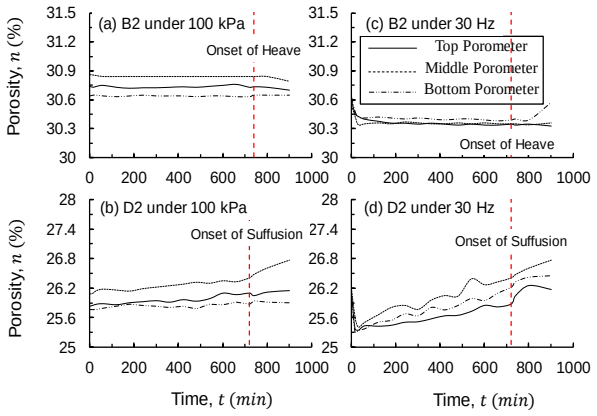

Fig. 8: Porosity variations for B2 and D2

5.2. Modified Criterion for Cyclic Loading Conditions

As discussed in the introduction, the original criterion of Indraratna et al. [9] compares D_{c35}^{c} of coarser fraction with $d_{85,SA}^{f}$ of finer fraction in order to assess the potential of internal instability. In the above criterion, D_{c35}^{c} is the only variable that may vary with the level of compaction and agitation due to cyclic loading [14, 27]. Given the constrictions may only vary between the loosest and the densest sizes depending upon the R_d of soil, which shows higher stability at $R_d \geq 95\%$. For instance, the current soils C1 and C2 during testing phase-I exhibited instability at $R_d \approx 5\%$, whereas the same soils showed internal stability at $R_d \geq 95\%$ during both phases-I and -II. In contrast, the same soils C1 and C2 at $R_d \geq 95\%$, exhibited internal instability due to agitation and pore pressure development under cyclic loading during phase-III. This clearly indicated that the loosest constriction sizes control the potential of internal instability under cyclic conditions [28]. Therefore, in order to assess the internal stability under cyclic conditions, it would be conservative to compare the controlling constriction size corresponding to $R_d = 0\%$, i.e. D_{c35}^{cl} with the $d_{85,SA}^{f}$. As shown by the predictions in the last column of Table 4, this proposed revision to the criterion of Indraratna et al. [9] agrees fully with the experimental results of phase-III (i.e. 100% success).

Table 5 presents the experimental data adopted from published literature for objective validation of the modified criterion proposed for cyclic conditions. A total of 30 data points adopted from 7 published studies including 2 from Alobaidi and Hoare [26], 4 each from Kabir et al. [24], Haque et al. [13], Trani [12] and Trani and Indraratna [19], and 6 each from Chung et al. [25] and Kamruzzaman et al. [23]. Notably, this data originated from various combinations of cyclic loads (σ_{min}' = 30 to 75 kPa and σ_{max}' = 70 to 145 kPa), frequencies (f = 2 to 15 Hz) and uniformity coefficients (C_u = 3 to 45) across 7 different research studies. Given the poor performances from the methods of Burenkova [7], Sherard [3] and Wan and Fell [8], only the methods of Indraratna et al. [9], Kenney and Lau [5] and Kezdi [2] were adopted for assessing the instability potential of this dataset in Table 5. In essence, the PSD based geometrical criteria of Kenney and Lau [5] and Kezdi [2] obtained 7 and 13 incorrect predictions, respectively, whilst the CSD based criteria of Indraratna et al. [9] resulted into only 4 inconsistent predictions. Nevertheless, none of these criteria could assess the correct

potential of internal instability with 100% accuracy. In contrast, the modified criterion of Indraratna et al. [9], proposed herein, could correctly capture the instability potential of all samples with a remarkable success rate of 100%.

6. Implications and Scope

In this study, the hydraulic tests were performed on cohesionless soils (i.e. sands, fine gravels, clay-silt-sand-gravel mixtures and sand-gravel mixtures). The current study possesses the following limitations:

1. The scale of laboratory specimens may not be comparable with most practical scenarios in the field, a limitation associated with most laboratory testing published so far,
2. Only a single magnitude of sinusoidal cyclic (heavy haul) loading was applied at 5, 10, 20 and 30 Hz loading frequencies during the cyclic tests, whilst normal stresses of 0, 25, 50 and 100 kPa were applied during the static tests. Notably, the loading conditions and magnitudes could be different from those simulated in this study, and
3. The relative density was kept above 95% during phases-II and III, however, the level of compaction of most practical filters may not be that high. The practical implications include the assessments of internal instability potential under static and cyclic loading conditions, e.g. embankment dam filters and railway subballast filters. The observed mechanisms of seepage induced failures can be useful for modelling the inception of internal instability in granular filters.

7. Concluding Remarks

The results are reported from a series of hydraulic gradient controlled filtration tests on six granular soils at different levels of compaction at 0 < Rd ≤ 100% and the following conclusions were drawn:

- The potential of internal instability is governed by the both particle size distribution and the level of compaction of soils. The risk of occurrence of internal instability can be significantly reduced by increasing the relative density of soils. In practice, the initial placement conditions offer greater control, whereby placing a densely compacted filter could effectively minimize the risks of occurrence of internal instability in unfavorable conditions.

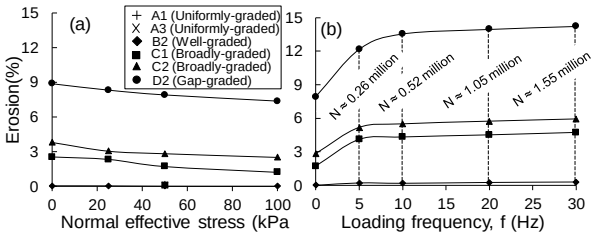

Fig. 9: Effects of (a) normal static load and (b) cyclic loading frequency on erosion

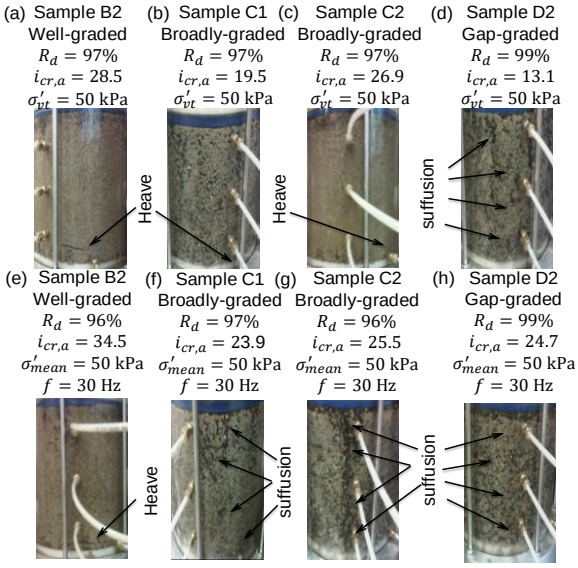

Fig. 10: Seepage failures observed in phases II and III

- Non-uniform broadly-graded (Cu > 10) and gap-graded soils possess higher potential of internal instability. These soils may suffer from internal erosion at relatively smaller hydraulic gradients than the uniform and well-graded soils (Cu < 10) that exhibit heave development at relatively larger critical hydraulic gradients.
- Increasing the magnitude of static loading could sufficiently reduce the internal erosion and increase the magnitude of critical hydraulic gradient for internal instability (e.g. Figs. 4 and 7a). For practical purposes, placing high magnitude surcharge over the downstream filters in embankment dams can be an effective measure for reducing the risk of piping. In contrast, the cyclic loading increases the risk of internal erosion in soils that becomes excessively premature at higher frequencies, as demonstrated in Fig. 7b.
- The existing PSD based methods show limited success in determining the potential for internal instability of filters subjected to static

loading, whilst the CSD based criterion showed 100% success. Not surprisingly, none of the existing criteria could successfully assess the internal instability potential of filters under cyclic loading. This may be because the repeated nature of cyclic loads causes the constriction sizes to fluctuate rapidly, thereby causing increased erosion. Nevertheless, by assuming Rd = 0% to discount the effects of cyclic conditions, the constriction based criterion could assess the internal instability potential of current samples under cyclic loading with enhanced accuracy.

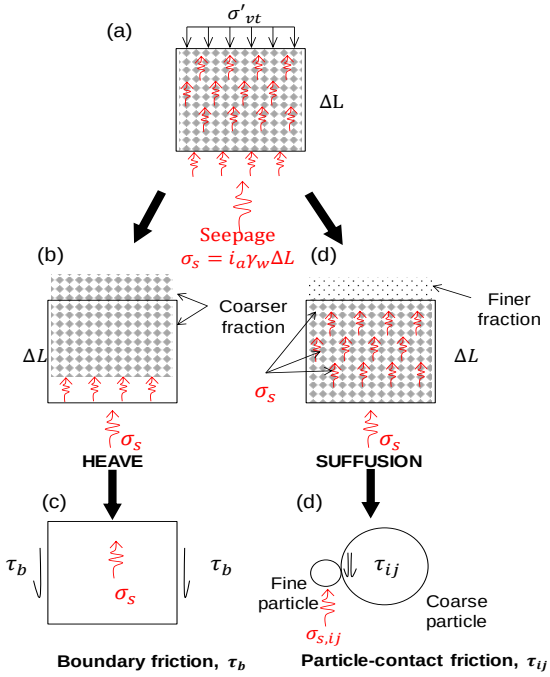

Fig. 11: Schematic illustration of mechanisms for seepage induced instability (i.e. heave and suffusion) in granular soils

- The analysis revealed that the soils with C_u < 10 exhibit higher internal stability under cyclic high frequency loading (e.g. soils A1, A2, A3, B1, and B2). Thus, soils with C_u < 10 should be preferred for protective filters to ensure longevity, internal stability and effectiveness under unfavorable hydraulic conditions, especially in railway substructures subjected to high speed train loading. In particular, uniform medium sands and fine gravels show enhanced internal stability under cyclic loading.

8. Acknowledgement

Fund from University of Engineering and Technology Lahore in the form of FDP scholarship is gratefully acknowledged.

9. References

[1] Unites States Army Corps of Engineers USACE. (1953). Investigation of filter requirements for underdrains. Technical Memorandum No. 3–360, U.S. Waterways Experiment Station, Vicksburg, Miss.

[2] Kezdi, A. (1979). Soil physics, Elsevier Scientific, Amsterdam, The Netherlands.

[3] Sherard, J. L. (1979). Sinkholes in dams of coarse broadly graded soils. Proceeding of 13th Congress on Large Dams, New Delhi, 2, 25-35.

[4] Terzaghi, K. (1939). Soil mechanics—A new chapter in engineering science. Institute of Civil Engineers 12(7), 106–142.

[5] Kenney, T. C., & Lau, D. (1985). Internal stability of granular filters. Canadian Geotechnical Journal 22, 215–225.

[6] Chapius, R. P. (1992). Similarity of internal stability criteria for granular soils. Canadian Geotechnical Journal 29(4), 711-713.

[7] Burenkova, V. V. (1993). Assessment of suffusion in non-cohesive and graded soils. Filters in geotechnical and hydraulic engineering, J. Brauns, M. Heibaum, and U. Schuler, eds., Bakema, Rotterdam, The Netherlands, 357-360.

[8] Wan, C. F., and Fell, R. (2008). Assessing the potential of internal instability and suffusion in embankment dams and their foundations. Journal of Geotechnical and Geoenvironmental Engineering, 134(3), 401–407.

[9] Indraratna, B., Israr, J., & Rujikiatkamjorn, C. (2015). Geometrical method for evaluating the internal instability of granular filters based on constriction size distribution. Journal of Geotechnical and Geoenvironmental Engineering 141(10), 1-14.

[10] Indraratna, B., Raut, A. K., & Khabbaz, H. (2007). Constriction-based retention criterion for granular filter design. Journal of Geotechnical and Geoenvironmental Engineering, 133(3), 266–276.

[11] Israr, J., Indraratna, B., & Rujikiatkamjorn C. (2016). Laboratory modelling of the seepage induced response of granular soils under static and cyclic conditions. Geotechnical Testing Journal 39(5), 1-18.

[12] Trani, L. D. O. (2009). Application of Constriction size based filtration criteria for railway subballast under cyclic conditions. PhD thesis, University of Wollongong, Wollongong, Australia.

[13] Haque, A., Kabir, E., & Bouazza, A. (2007). Cyclic filtration apparatus for testing subballast under rail track. Journal of Geotechnical and Geoenvironmental Engineering, 133(3), 338–341.

[14] Locke, M., Indraratna, B., & Adikari, G. (2001). Time-dependent particle transport through granular filters. Journal of Geotechnical and Geoenvironmental Engineering 52(6), 521-529.

[15] Israr, J., & Israr, J. (2018). Laboratory modelling and assessment of internal instability potential of subballast filter under cyclic loading. Pakistan Journal of Engineering and Applied Sciences, 22(1), 72-80.

[16] Israr, J., & Israr, J. (2018). Experimental investigation and assessment of internal stability of granular filters under one-dimensional static and cyclic loading. Geotechnical Testing Journal, 41(1), 103-116.

[17] Skempton, A. W., & Brogan, J. M. (1994). Experiments on piping in sandy gravels. Geotechnique, 44(3), 449–460.

[18] Das, B. M. (2008). Advanced Soil Mechanics, Taylor & Francis, London, UK.

[19] Trani, L. D. O., & Indraratna, B. (2010). Assessment of Subballast Filtration under Cyclic Loading. Journal of Geotechnical and Geoenvironmental Engineering 136(11), 1519-1528.

[20] Israr, J. (2016). Internal instability of granular filters under cyclic loading. PhD thesis, University of Wollongong, Wollongong, Australia.

[21] Zou, Y., Chen, Q., Chen, X., & Cui, P. (2013). Discrete numerical modelling of particle transport in granular filters. Computers and Geotechnics, 32(5), 340–57.

[22] Israr, J., & Indraratna, B. (2017). Internal stability of granular filters under statc and cyclic loading. Journal of Geotechnical and Geoenvironmental Engineering 143(6), 04017012.

[23] Kamruzzaman, A. H. M., Haque, A., & Bouazza, A. (2008). Filtration behaviour of granular soils under cyclic load. Geotechnique 58(6), 517–522.

[24] Kabir, E., Haque, A., & Bouazza, A. (2006). Influence of cyclic load on the design of Subballast. Poceedings of the Conference on Railway Engineering, Melbourne, 181-184.

[25] Ip, C. M., Haque, A. & Bouazza, A. (2012). Influence of cyclic stress pulse shapes on filtration behaviour of railway subballast. Journal of Geotechnical and Geoenvironmental Engineering 138(2), 230-235.

[26] Alobaidi, I. M., & Hoare, D. J. (1998). Qualitative criteria for anti-pumping geocomposites. Geotextiles and Geomembranes, 16(4), 221-245.

[27] Xiao, M., Reddi, L. N., & Steinberg, S. (2006). Effect of vibrations on pore fluid distribution in porous media. Transport in Porous Media, 62(2), 187-204.

[28] Indraratna, B., Israr, J., & Li, M. (2018). Inception of geohydraulic failures in granular soils-an experimental and theoretical treatment. Geotechnique, 68(30, 233-248.